DOR: 20.1001.1.2322388.2019.7.2.5.9

Research Paper

Fabrication of the Ordered Nanocells of Anodic Aluminum Oxide and the Generation of Zn-Mn Ferrite Phase within Them

Masoud Soltani[1*], Zeinab Erfani Gahrouei[1], Saeed Akhavan[1], Ali Shafyei[2]
1. M.Sc., Department of Materials Engineering, Isfahan University of Technology, Isfahan, Iran
2. Peofessor, Department of Materials Engineering, Isfahan University of Technology, Isfahan, Iran

ARTICLE INFO

Article history:

Received 5 February 2019
Accepted 27 April 2019
Available online 1 May 2019

Keywords:
Anodizing
Temperature
Nanocells
Ferrite
Magnetic

ABSTRACT

Different ceramic coatings can be fabricated on aluminum alloys by the anodizing process. In this process, the nanocells can grow directly from the bottom toward the surface of the coating layer. The ordered porous structure of the anodic aluminum oxide (AAO) layer is a very suitable template for the growth of magnetic nanowires. At this study, one- and two-step anodizing processes were conducted to fabricate the oxide layer in an appropriate acidic electrolyte at three different temperatures (0, -5, -10 ^{0} C) and three different voltages (20, 27, 35 V) for 50 min on a 7075 aluminium alloy (7075 AA). The results showed that the samples' thickness increased with increasing the voltage and decreasing the temperature. The microhardness of samples under different voltages increased with decreasing the temperature. Field emission scanning electron microscopy (FESEM) images were taken from the back and cross-sections of nanocells. The results indicated that the samples which were anodized by the two-step process at -10 ^{0} C and 35 V had yielded the best order. Afterward, Zn-Mn ferrite nanowires were produced by electrochemical deposition within the nanocells. X-ray diffraction (XRD) confirmed the formation of the Zn-Mn phase, and FESEM images showed the bulk morphology of nanowires with an appropriate saturation magnetization of about 63.64 emu/g.

[*] **Corresponding Author:**
Email Address: m.71.soltani@gmail.com

1. Introduction

Anodizing is an electrochemical process in the acidic electrolyte, which has been used for improving the mechanical and corrosion behavior and decoration of aluminum alloys since 1923. The oxide coating of the anodizing process is comprised of two layers. The first layer is in direct contact with the aluminum substrate, free of porous and holes, which is called the barrier layer. The second one has ordered nanoporous, and its structure is like hexagonal columns with tube-like holes in the center, which grew from the bottom to the surface of the coating layer [1-3].

Several studies have been conducted in order to investigate the effect of different parameters such as the type of electrolyte, time, voltage, temperature, and the type of anodizing current on the structure, performance, and ultimate properties of coatings [4-6]. In recent years, incorporating particle reinforcements into the oxide layer and fabricating different composites have been studied in order to improve the surface properties of aluminum alloys [7-11]. Moreover, AAO has attracted a lot of attention to be used as a template for the growth and generation of different materials using various methods [12]. The cell order is a very important factor for the better incorporation of materials into the oxide layer [13]. Consequently, the investigations move toward fabricating an AAO layer with the highest order [13-18]. There are two methods for the production of second phase and different materials within an AAO layer: (1) wet chemical techniques including self-assembled monolayers [19], polymer modification [20], sol-gel [21-24], electroless deposition [25, 26], and electrochemical deposition [27], (2) gas-phase technique including thermal vapor deposition [28], atomic layer deposition [29], plasma polymer deposition [30], and chemical vapor deposition [31]. Among them, electrochemical deposition can be a very suitable method due to its simplicity, low-cost equipment, and special conditions (like a vacuum) [32]. Silver-gold [33], cobalt [34], iron-cobalt [35], nickel [36], iron [37], nickel-phosphorous [38] and other types of nanowires, with magnetic properties, have been grown within an AAO template [39].

Zn-Mn ferrite is used in memory chips, magnetic recorder media, transformers cores, radio-frequency coil fabrication, and many branches of telecommunication and electric engineering due to its good magnetic properties and ease of production [40]. Therefore, by depositing this magnetic spinel within an ordered AAO layer using electrochemical deposition, it is possible to simultaneously take advantage of the properties of the Al anodized layer and magnetic characteristic of Zn-Mn ferrite in aircraft.

In this study, the one-step anodizing process was firstly carried out at different temperatures and voltages in a specific electrolyte and at a specific time. Thickness, hardness, roughness, and the order degree of oxide coatings were examined, and the effect of two-step anodizing on the order of nanocells was also investigated. Then, Zn-Mn ferrite magnetic phase was generated within the nanocells with the highest order by electrochemical deposition and was characterized accurately.

2. Experimental Procedure

2.1 Substrate preparation

7075 AA with a chemical composition (wt%) of 89.31% Al, 5.6 %Zn, 2.31 %Mg, 1.53 %Cu, 0.57 %Fe, 0.43 %Si, and 0.25 %Mn was used as a substrate. The samples were prepared as disks with a diameter of 12 mm and a thickness of 1 mm. Then, they were grounded by emery paper 80 to 4000 and polished by 1 µm alumina powder.

Surface contaminants and lipids can have a negative impact on adherence between the coating and substrate [41]. To ensure that all the contaminants and lipids are removed, the substrates were immersed in a NaOH bath with saturated dissolved Al at 50 ^{0} C for 3 min. To activate the surface, the substrates were immersed in 30 wt% nitric acid solution at ambient temperature for one min.

2.2 Anodizing

For anodizing, a special Teflon corrosion-resistant reactor was used. An Al plate and the sample, as a cathode and anode, respectively, were placed within the chamber, and the device plugged into a DC supply power. The distance between the cathode and the anode was 2.5 cm. To decrease the temperature, the reactor was placed in a Lauda cooling bath. 165 g/l sulfuric acid and 10 wt% sulfosalicylic acid were used as the electrolyte. Coating time was performed in 50 min. Other coating conditions and the sample's code are shown in Table 1. To investigate the effect of two-step anodizing on the nanocells order, both the one- and two-step anodizing was conducted. To conduct this process, the samples were anodized for 40 min under the conditions shown in Table 2, and then the samples were immersed into a bath which its details are shown in Table 3, in order to remove the fabricated coating layer. After removing the initial coating layer, final coats on the substrate were fabricated under previous conditions.

Table 1. One-step anodizing conditions and the sample's code

-10	-5	0	Temperature (℃) / Voltage (V)
A1020	A0520	A0020	20
A1027	A0527	A0027	27
A1035	A0535	A0035	35

Table 2. Two-step anodizing conditions and the sample's code

-10	-5	0	Temperature (℃) / Voltage (V)
B1020	B0520	B0020	20
B1027	B0527	B0027	27
B1035	B0535	B0035	35

Table 3. Condition of oxide layer removing after the first step anodizing

Time (min)	Temperature (℃)	Solution
10-20	70	1.8 % Wt Cr_2O_3 + 6 % Wt H_3Po_4

2.3 Generation of Zn-Mn ferrite magnetic layer

The barrier layer can prevent the proper growth of the nanowires during the electrodeposition process due to its insulating nature [34-36]. So, this layer was thinned by a voltage reduction with a rate of 2 volts per minute. The solution used for deposition is comprised of 0.048 molar $Mn(NO_3)_2$, 0.016 molar $Zn(NO_3)_2.6H_2O$, and 0.05 molar $Fe(NO_3)_3.9H_2O$. The electrochemical deposition was conducted at ambient temperature using a two-electrode system, in which the sample and a platinum plate were used as cathode and anode, respectively.

2.4 Characterization

To examine the crystal structure of the samples with AAO coating and to ensure the formation of Zn-Mn ferrite phase on AAO, the X-ray diffraction (XRD, model Philips X'pert MPD) test was performed. To avoid the influence of Al substrate and AAO on the peaks obtained during the characterization of Zn-Mn ferrite, both of them were removed from the spinel coat, and only the spinel was examined. To have a closer investigation on the crystal structure of AAO coat, the Grazing Incidence X-Ray Diffraction (GIXRD) test was performed on the surface of the coat. This test was conducted by PANalytical-XPert PROmpd with monochromatic light, similar wavelength, time steps of 90 sec, degree of 0.04, and the diffraction angle of 2 to 90°.

The thickness of coatings fabricated under different coating conditions in one-step anodizing was measured using an eddy current-based thickness gauge (model CEM DT-156). The hardness of samples fabricated by one-step anodizing was measured by a Wilson 402MVD microhardness apparatus with a load of 200 gr and a dwelling time of 20 sec. The roughness of samples fabricated by one-step anodizing was measured by a stylus roughness tester (model Mitotoyo SJ.210) for a length of 5 mm.

To investigate the order degree of generated nanocells from two sides, the back and the cross-sections of coatings were examined by a Hitachi-S4160 field emission scanning electron microscope. To do so, the samples were placed on thin glass. Then, they were immersed into a saturated solution of CuSO4 at room temperature for the Al substrate to be removed, and a coating with several microns remains. Moreover, to observe the columnar arrangement of nanocells, the samples were cut by a special saw and then broken, for the un-polished broken surface, within which nanocells can be seen, be examined. After that, the samples were placed on a holder, and the images were taken.

Magnetic measurements were carried out by a vibrating sample magnetometer (VSM), Lake Shore 728 model. Samples were prepared by packing the magnetic phase into pellets. Magnetization curves were recorded at room temperature (300 K).

Saturation magnetization (Ms) values were extrapolated from the high field part of the measured magnetization curves, where the magnetization increases linearly with 1/H, when it tends to be zero.

3. Results and discussion

3.1 Analysis of AAO coatings

Fig. 1 shows the XRD pattern of the AAO surface for the A1035 sample. A hill between the angle of 20 and 30 indicates the amorphous structure of the coating layer fabricated by anodizing in sulfuric acid and generally in all acidic electrolytes [42]. XRD analysis software shows that the emerged peaks are most likely related to Al substrate. The diffraction patterns related to FCC Al can be seen on each peak. Due to the large thickness of the coating layer, the presence of the Al peak is not expected. AAO formed in the acidic electrolyte has an amorphous structure [43]. Therefore, it is expected that X-ray has passed this structure and reached the Al substrate [44]. Otherwise, some amount of Al substrate has been entrapped within the coating layer during anodizing. The entrapment possibility of free Al within the coating layer is small. XRD test with a small X-ray incident angle was performed to see if the X-ray has passed the coating layer. Fig. 2 shows this pattern from the angle of 2 to 90°. It can be seen that there is not an observed peak, and only the hill resulted from the angle between 10° and 30° is observed, which confirms the amorphous structure of the coating layer. As a result, if a high-angle and near-to-right angle X-ray incident reaches the surface of AAO coating, even if the coating thickness is high due to the amorphous structure, the X-ray incident passes through the coating layer and reaches the substrate. In general, to obtain precise information associated with this coating layer, the X-ray incident should reach the surface at a small angle.

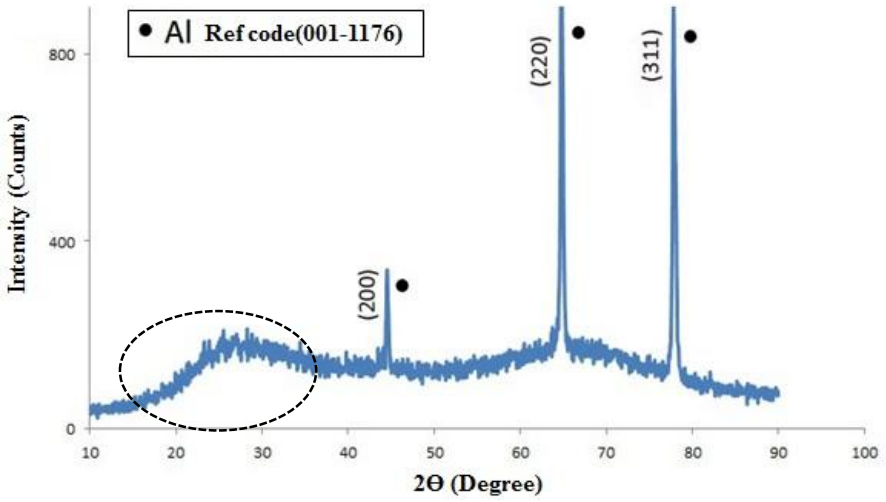

Fig. 1. XRD pattern of A1035 sample.

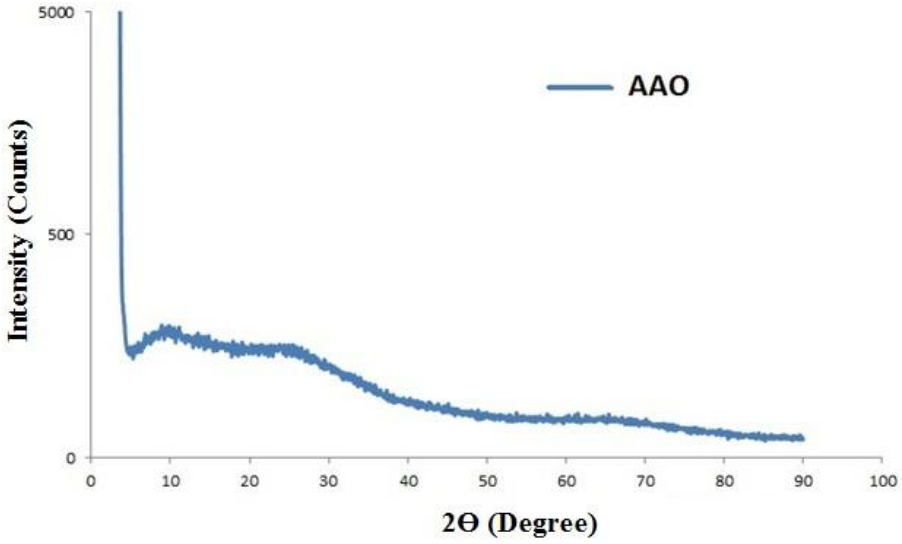

Fig. 2. GIXRD pattern of A1035 sample.

3.2 The thickness of AAO coatings

The results of coating thickness are shown in Fig. 3. The maximum thickness is related to the sample which is anodized at -10 ^{0}C under 35 V, whereas the minimum thickness is related to the anodized sample at 0 ^{0}C under 20 V. This shows that increasing the voltage and decreasing the coating temperature at the same time would significantly increase the coating layer thickness. The thickness of the anodized sample at 20 V has not significantly increased with decreasing the temperature, and its thickness has increased by 10 µm, whereas the thickness of the anodized sample at 35 V has increased by 21 µm with temperature reduction. Therefore, it can be concluded that if the temperature decreases and the voltage is not as high as enough, the thickness will not increase considerably. In fact, for increasing the thickness, both optimum temperature and voltage are essential [45-47].

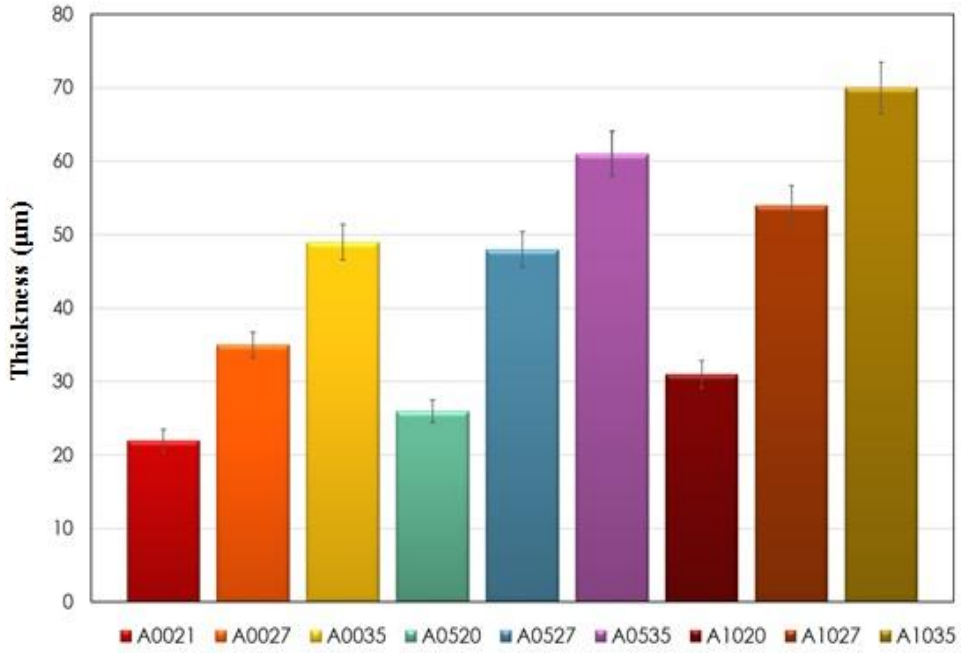

Fig. 3. Thickness of coating layers after one-step anodizing.

3.3 Hardness and roughness of AAO coatings

As can be seen in Fig. 4, the highest hardness value at each constant temperature was obtained for the voltage of 27 V. It should be noted that the considered values in Fig. 4 are the average of ten hardness values measured on different points of the coating layer. It can be seen that the increased microhardness against voltage does not follow a constant rule. At all temperatures, with increasing the voltage, the microhardness firstly increases and then decreases, so the microhardness of the coating layer fabricated at 35 V has decreased compare to the ones fabricated at 27 V. In fact, at constant time, the current density reduces significantly after reaching a specific voltage, which in turn, the excess of voltage is used for enlarging the nanoholes which form during the anodizing process and decreases the microhardness [44, 47, 48]. Moreover, the reduction of temperature increases the coating layer's hardness and is not dependent on the voltage. In other words, the solubility of the electrolyte decreases with decreasing the temperature and results in the porosity reduction of the coating layer [49].

The hardness value of the coatings formed at 20 V at each temperature is less than 500 Vickers. This shows that the process done under 20 V at any given temperature, even if it is suitable, does not result in obtaining a high hardness value. As a result, higher voltage is needed in order to reach higher hardness for the anodized sample. Therefore, there is an optimum value between coating temperature and voltage with microhardness, and the optimum sample is A1027 sample with a coating layer thickness of 54 µm.

AAO coating is hard and cannot show significant plastic deformation, and its deformation is mainly elastic [50]. Hence, after applying a load on the sample, the roughness can have a considerable effect on the way the applied stress is distributed on the coating layer and the substrate. Moreover, the more the roughness is, the more the adsorption ability and the adherence of the coatings are subsequently applied [51]. Therefore, the roughness

of these coatings is an effective parameter for the coating properties. The results of the roughness of the coating are shown in Table 4. As can be seen, with decreasing the temperature and increasing the voltage, the surface roughness increases. As a result, the harder the surface is, the more the surface roughness and the absorbing ability.

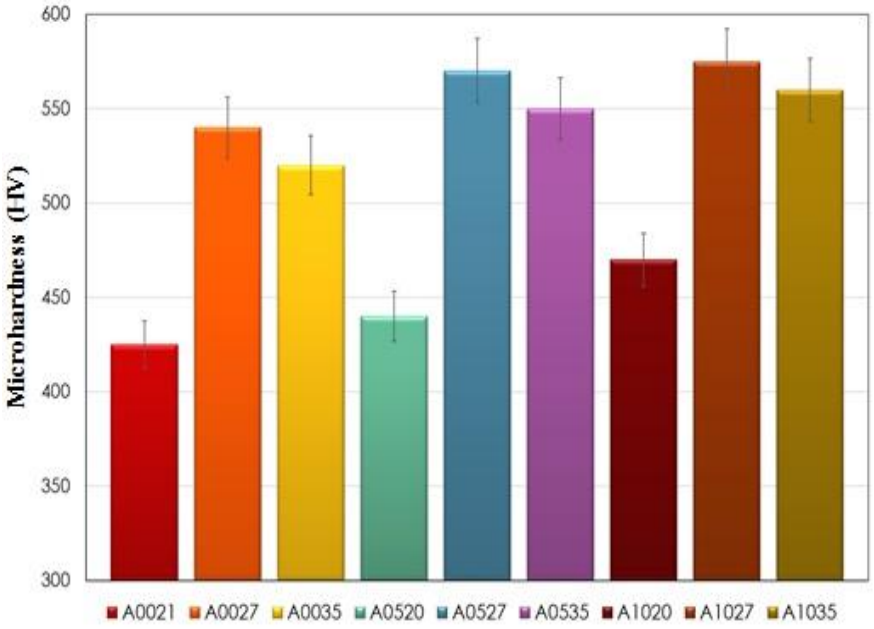

Fig. 4. Microhardness of coating layers after one-step anodizing.

Table 4. Surface roughness data for the oxide coatings after one-step anodizing

A1035	A1027	A1020	A0535	A0527	A0520	A0035	A0027	A0020	
1.43	1.29	1.24	1.39	1.25	1.21	1.31	1.19	1.16	R_a (µm)
1.82	1.78	1.69	1.74	1.71	1.48	1.68	1.55	1.52	R_q (µm)
10.32	10.21	9.91	10.23	9.87	8.52	10.27	9.93	9.81	R_z (µm)

3.4 Investigation of the ordered AAO coatings

As can be seen in Fig. 5a, the nanocells are not generated from the bottom to the surface of the coating layer with sufficient order at zero temperature and 20 V. The columns are not also columnar and are inclined. The diameter of nanocells is ranged from 33 to 98 nm (this value is measured by Image J software), which is a significant difference, and as a result, the structure does not have a desirable order. Increasing the voltage to 27 V at zero temperature improves the order of nanocells because in fact, it increases the movement ability of Al^{3+} ions in the electrolyte, and therefore, the columns have a small inclination (Fig. 5b) [52]. The minimum and maximum diameters of the nanocells are 52 and 109 nm, in which the difference between the minimum and maximum diameter has decreased. With increasing the voltage to 35 V (A0035), its order has increased compared to A0020 and A0027 samples because the columns have grown in a columnar form (Fig. 5c). But it can be seen that the growth is not complete, and the nucleation in the bottom of nanocells is disordered in some regions. The minimum and maximum diameters of the nanocells are 54 and 97 nm, which the difference has decreased in comparison with the A0020 and A0027 samples. In the same way, increasing the voltage at the other two temperatures increases the order of templates.

By comparing the images taken from the cross-section of the coatings fabricated at -5 ^{0}C (B0535, B0527, B0520), it is obvious that under two-step anodizing, increasing the voltage increases the order of templates (see Fig. 5d-f). The puffy structure in some regions of B0520 coating's cross-section (Fig. 5d) is due to the low applied voltage at -5 ^{0}C. In this case, the ions have a slight movement

ability and prevent the AAO structure from being smoothed. The nanocells order increases significantly with increasing the voltage to 27 V in a way that the puffy structure of the nannocells has decreased considerably (Fig. 5e). Finally, it seems that if the voltage is adjusted at 35 V, the template order reaches its best form at -5 ^{0}C (Fig. 5f).

The less the temperature, the less the movement ability of ions in the electrolyte, and so the ions cannot reach the desired site [49]. When the movement speed of ions decreases, their shearing ability reduces and cannot eliminate the disordered layers during the growth process, and a smooth and flat wall is formed. On the other hand, when the movement speed of ions decreases, they cannot penetrate into the depth of nanocells and form an AAO phase with an ordered structure [48, 53]. It is also possible that, due to the lack of sufficient speed, ions stick to the coating wall and decrease the order significantly [53]. Therefore, for the ions at low temperatures, a high voltage is needed to move orderly. High voltage increases the potential difference, and the current applied to ions [44, 51]. Hence, the ions move faster, reach the final destination, and the order increases. Therefore, when the coating voltage is 20 V, the temperature reduction decreases the movement of the ions. But because the voltage is not high enough, the template order decreases significantly. For this reason, A1020 has the lowest order (Fig. 5g). When the coating voltage is 27 V (Fig. 5h), due to the increased ability of ions movement, the temperature reduction has not had a significant effect on nanocell order as much as the effect of temperature reduction on the samples coated at 20 V. At 35 V, the temperature reduction increases the template order because it, in fact, decreases the corrosion ability of electrolytes, and if the voltage can supply the movement ability of ions, a highly-ordered structure can be obtained. For this reason, the best template order has been obtained at -10 ^{0}C and 35 V (as seen in Fig. 5i, 5j).

By examining and comparing the images of one- and two-step anodizing in Fig. 5, it is clear that the two-step anodizing has a considerable effect on the order of samples in comparison with one-step anodizing under all conditions. The reason is that when the nuclei of AAO are formed and grown, the barrier layer, which forms at the end of the coating layer (Fig. 6), is like a crescent formed on the Al substrate. As a result, the obtained structure is rough and has asperities [54].

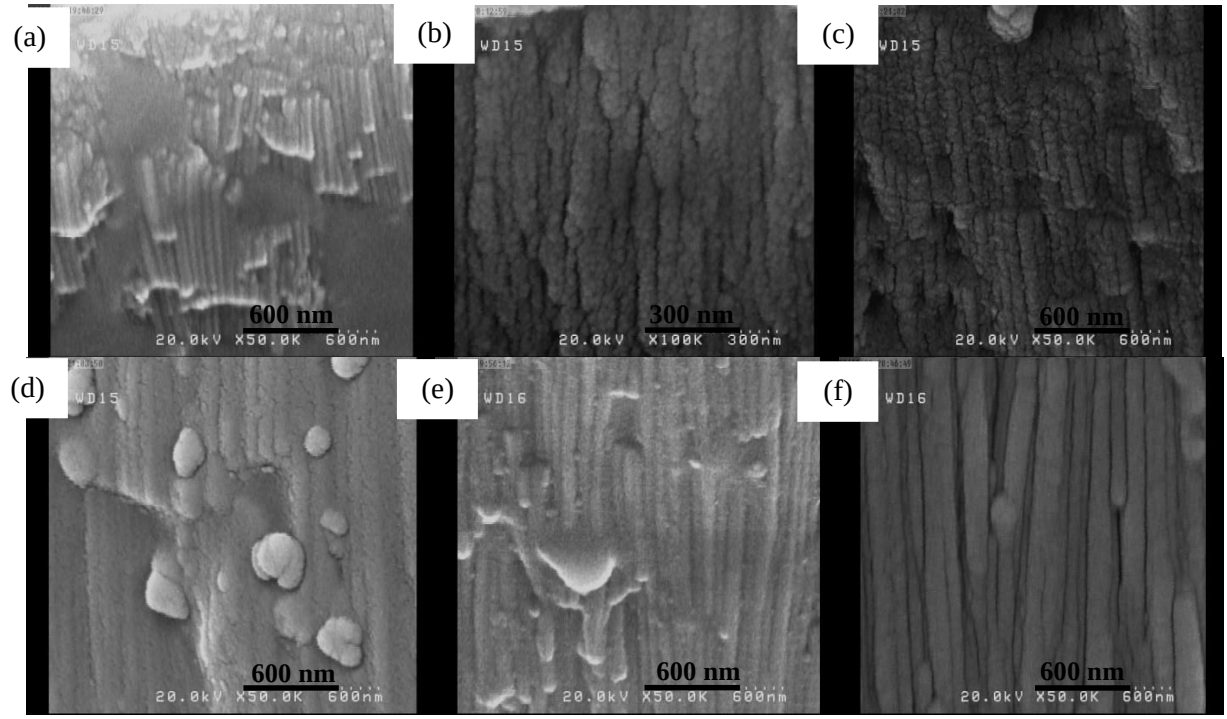

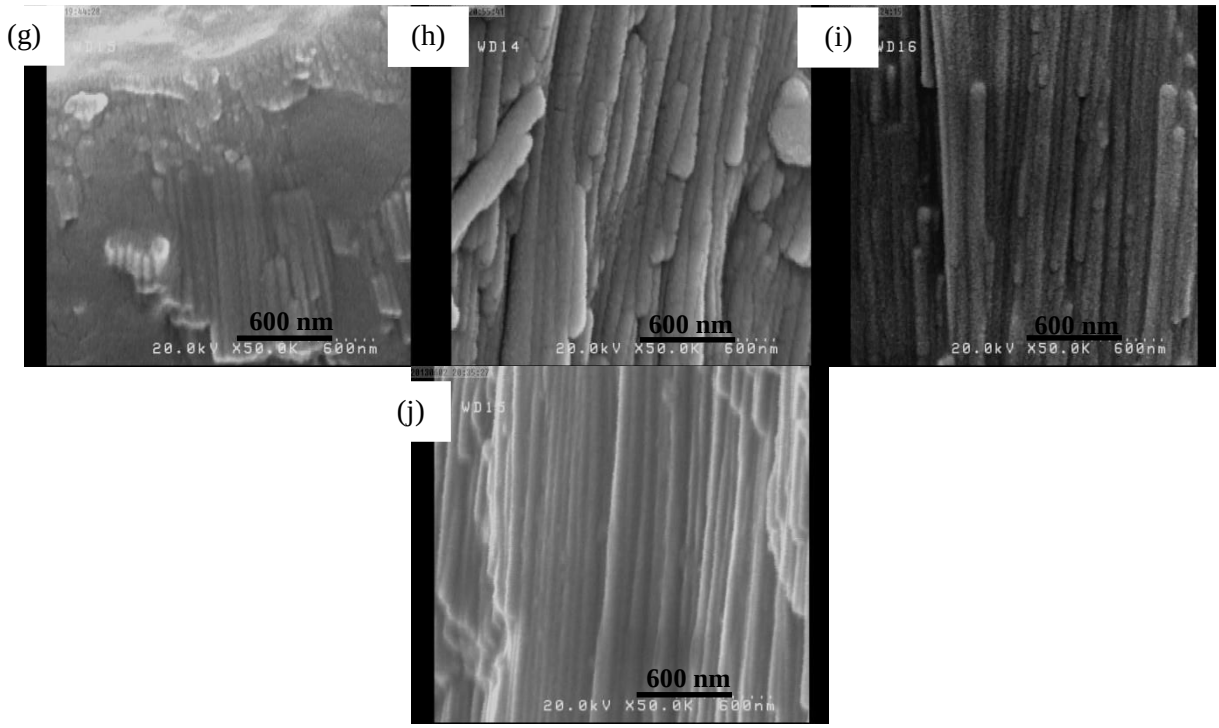

Fig. 5. FESEM images of nanocells from cross section of sample: a) A0020, b) A0027, c)A0035, d)B0520, e) B0527, f)B0535, g) A1020, h) A1027, i) A1035, j) B1035.

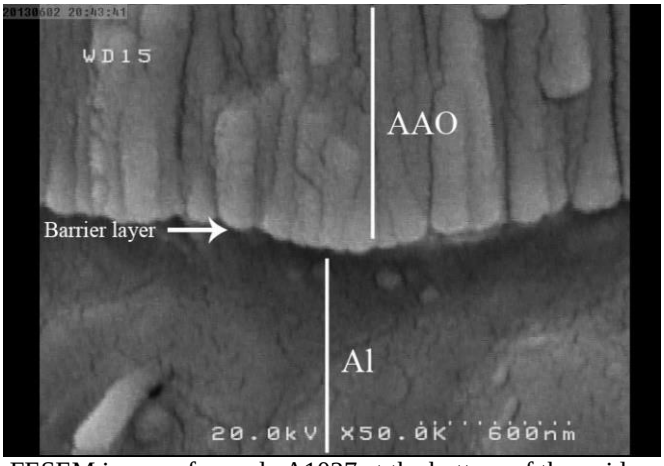

Fig. 6. FESEM image of sample A1027 at the bottom of the oxide coating.

After the first step of anodizing, when the generated AAO layer at first step is eliminated, the rough structure related to Al substrate remains, and during the second step of anodizing, the nucleases of AAO are grown on the asperities. The structure has a better order, and consistent growth continues to the end of the anodizing process due to the growth of these nucleases on this pattern. So, if the voltage and temperature are suitable (B1035), the columns are formed without inclination and with similar sizes (small differences). Note that the nanocell fractures in Fig. 5j are not related to the renucleation since the top part of the barrier layer is not like a hemisphere, and it is more like a part detached from the coating layer, which is in the same direction with the fracture direction of the coating layer. The images are taken from the back of nanocells (Fig. 7) show that there is a smaller empty space between the nanocells and ordered hexagonal cells in a two-step process (Fig. 7a-b) rather than the one-step process (Fig. 7c-d). As the barrier layer or the hexagonal cells are formed at the beginning of the coating process, the voltage does not have a significant effect on this layer [55]. But the more the thickness, the more the effect of voltage on the order degree of nanocells. Finally, it seems that B1035 can be chosen as a template for generating the magnetic phase because of its best order.

3.5 Structural characterization of Zn-Mn ferrite

Zn-Mn ferrite has a magnetic spinel structure. Fig. 8 shows the XRD result indicating the formation of Zn-Mn ferrite. All the XRD peaks are related to the spinel phase without any impurity and they are matched with $Zn_{0.4}Mn_{0.6}Fe_2O_4$. During the electrodeposition process, a magnetic layer is formed on the AAO layer, which doesn't allow the nanowires to be recognized. As a result, samples are polished in order to make them visible. The nanowires grow in a path to fill the nanocells completely and even cover them up. The nanowires stood out of the holes, because there is no barrier among them. At this time, synthesized nanowires are attached to each other and they grow continuously. Consequently, the images which were taken from the top of this structure are bulky (Fig. 9a). At higher magnification, the nanowires can be seen obviously (Fig. 9b).

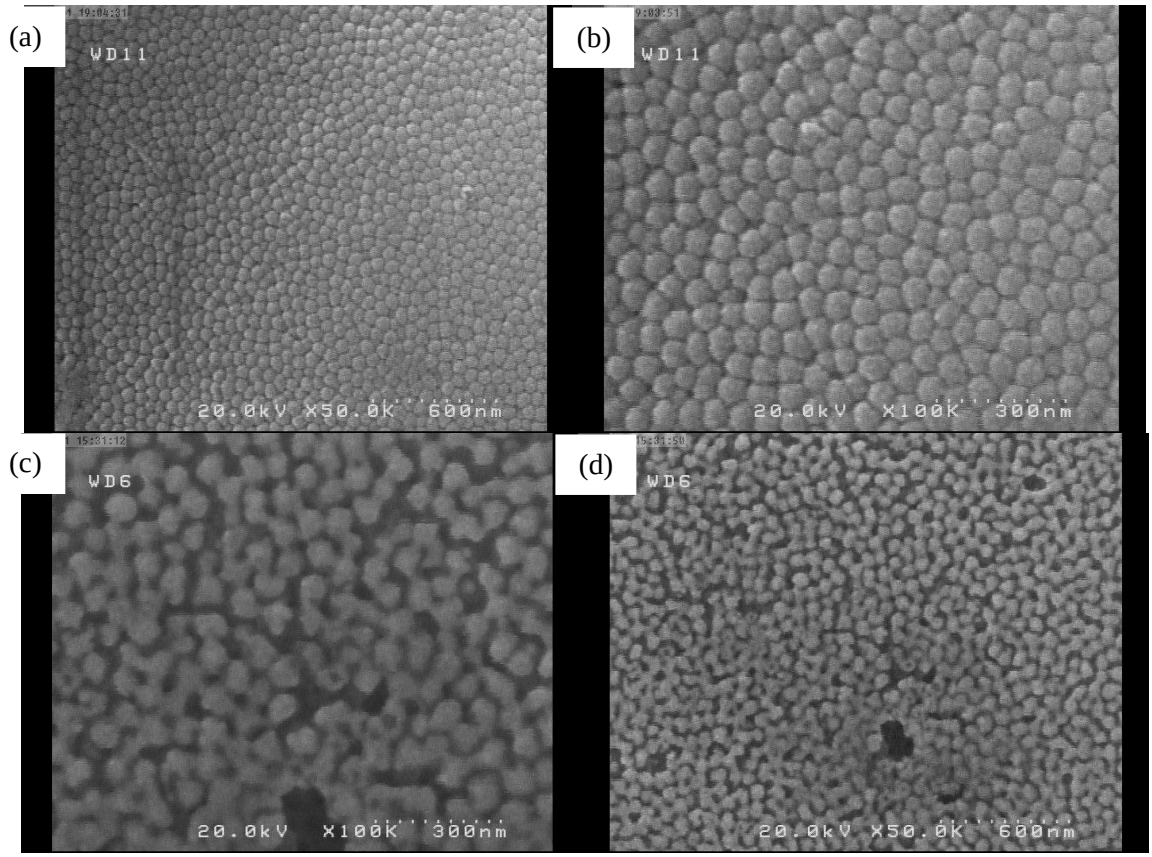

Fig. 7. FESEM images of nanocells from the back of the samples: a, b) B1035 and c, d) A1035.

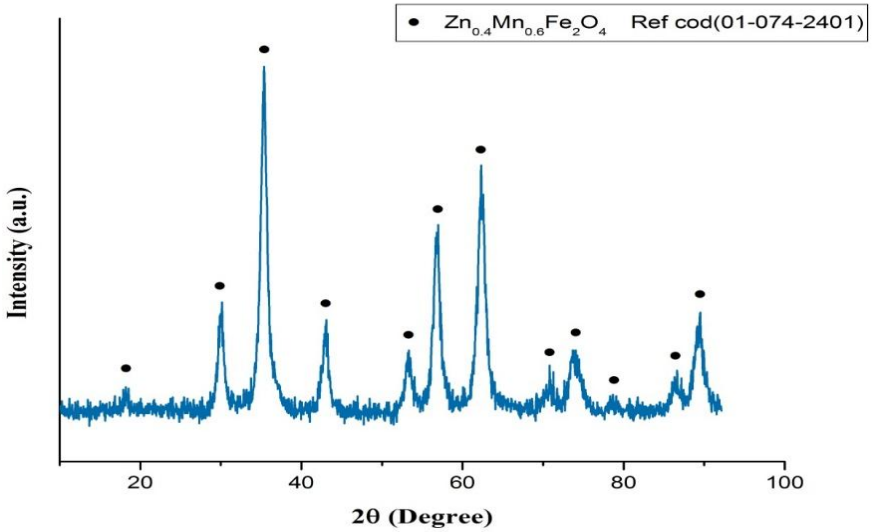

Fig. 8. XRD pattern of Zn-Mn ferrite layer.

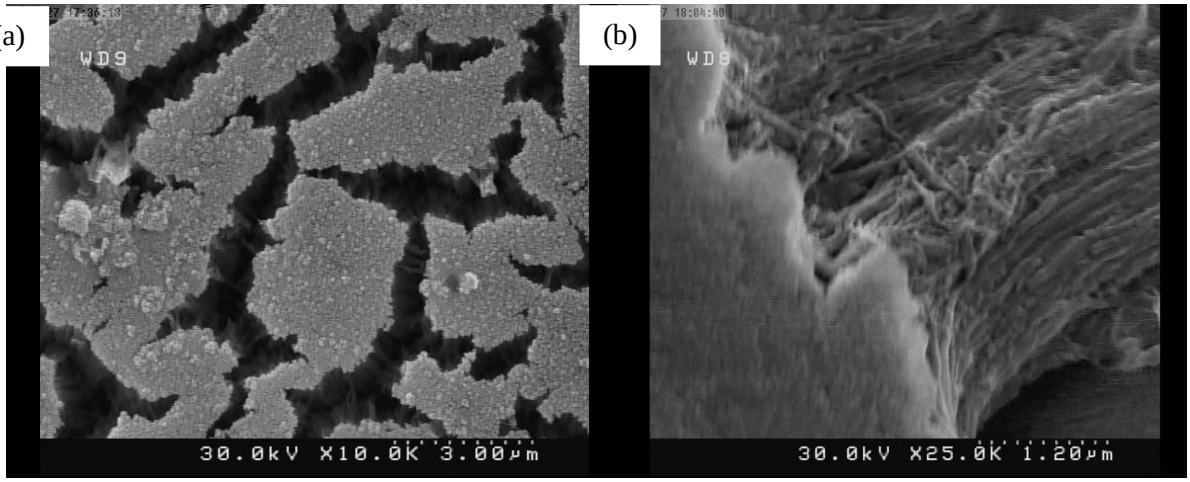

Fig. 9. FESEM images of Zn-Mn Ferrite layer at two different magnifications: a) 10000x and b) 25000x.

3.6 Magnetic properties of Zn-Mn ferrite

Fig. 10 shows the M-H curve of nanowires at ambient temperature. Magnetic properties obtained from the M-H curve are listed in Table 5. As can be seen in Fig 10, the coercivity of this sample is remarkable, and it reveals that these nanowires are hard magnetic materials. In fact, by removing an external magnetic field, magnetic properties remain in the sample, making them good candidates for different applications, such as MRI, catalysis, and photoelectronic and magnetic recording [56-59]. Moreover, these nanowires have high saturation magnetization, which is an important parameter for magnetic applications.

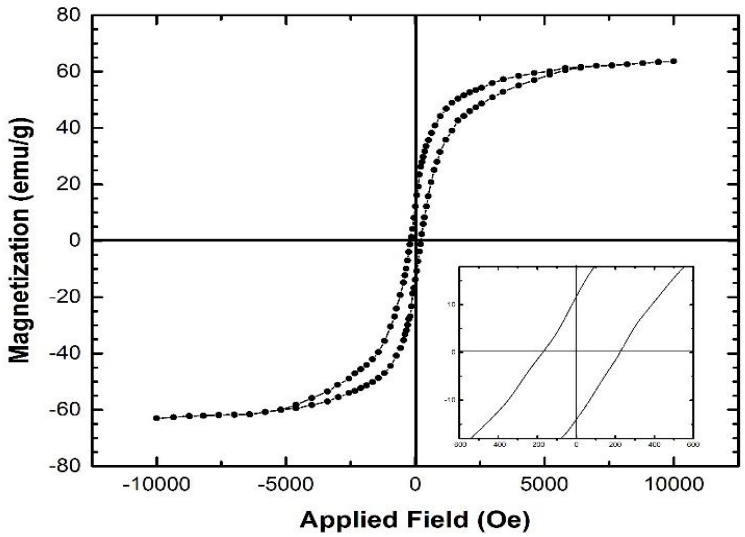

Fig 10. M-H curve of the synthesized nanowires at room temperature.

Table 5. Magnetic properties of Zn-Mn nanowires

Sample	M_s (emu/g)	M_r (emu/g)	H_c (Oe)	$R_s=M_r/M_s$
nanowires	63.64	13.86	230	0.22

According to the Stoner-Wohlfarth model, the Rs values of all samples are well below the ratio of 0.5, which could be characteristic of single domain nanowires at room temperature. So, if the ratio being slightly above 0.5, it means that samples are multi-domain nanowires that are randomly oriented and/or non-interacting nanowires having magneto crystalline anisotropy [60]. A comparison between the present work and other studies has been presented in Table 6, which shows that these nanowires have higher saturation magnetization than previous studies. In addition, these nanowires have sufficient coercivity for magnetic recording. According to magnetic results, synthesized nanowires can be used for a wide range of applications such as aircraft.

Table 6. Summary of magnetic properties of different samples in previous studies

Sample	Method	M_s (emu/g)	H_c (Oe)	Reference
$MnFe_2O_4$	Hydrothermal	62.07	78.91	[61]
$MnFe_2O_4$	Thermal deposition	45.9	-	[62]
$MnFe_2O_4$	Electrodeposition using AAO template	0.004	< 1	[63]
$ZnFe_2O_4$	Thermal deposition	15.7	< 1	[64]
$BaFe_{12}O_{19}$	Sol-gel using AAO template	56.14	5721.7	[65]
$CoFe_2O_4$	Electrodeposition using AAO template	~ 1	1900	[66]
Zn-Mn ferrite	Electrodeposition using AAO template	63.64	230	This work

4. Conclusion

- In this study, 7075 AA was anodized under different conditions, and the obtained oxide coating layer was characterized entirely. Furthermore, the possibility of magnetic spinel phase formation by electrochemical deposition within the AAO nanocells was studied. The conclusions are as follows:
- At all temperatures, increasing the voltage increased the thickness of AAO, and this was more effective at lower temperatures.
- At all temperatures, there is an optimum level between coating voltage and microhardness, but increasing the voltage increased the roughness at all three temperatures.
- The temperature reduction yields a better nanocell order if the voltage increases simultaneously. If the temperature decreases but the voltage does not increase simultaneously, the nanocell order is low due to the low energy of ions and speed of reactions.
- It is possible for Zn-Mn ferrite spinel to be formed on an AAO layer by using electrodeposition, and the bulks of Zn-Mn magnetic nanowires, which have stood out of nanocells are obtained.

References

[1] A. Santos, L. Vojkuvka, J. Pallarés, J. Ferré-Borrull, L. Marsal, "In situ electrochemical dissolution of the oxide barrier layer of porous anodic alumina fabricated by hard anodization", J. Electroanal. Chem. Vol. 632, No. 1-2, 2009, pp. 139-142.

[2] H.-s. Kim, D.-h. Kim, W. Lee, S.J. Cho, J.-H. Hahn, H.-S. Ahn, "Tribological properties of nanoporous anodic aluminum oxide film", Surf. Coat. Technol. Vol. 205, No. 5, 2010, pp. 1431-1437.

[3] M. Yoshimoto, Y. Morizono, S. Tsurekawa, T. Baba, "Anodizing of aluminum in sulfuric acid and oxalic acid solutions with percarboxylic acid-based additive", J. Ceram. Soc. Japan. Vol. 120, No. 1403, 2012, pp. 276-279.

[4] A. Brudzisz, A. Brzózka, G.D. Sulka, "Effect of processing parameters on pore opening and mechanism of voltage pulse detachment of nanoporous anodic alumina", Electrochim. Acta Vol. 178, No. 2015, pp. 374-384.

[5] S. Huang, B. Jiang, C. Liu, Q. Shao, H. Li, "Effect of negative current on the microstructure of oxide coatings prepared by hybrid pulse anodization", Metals. Vol. 9, No. 1, 2019, pp. 22.

[6] Y. Wong, M. Affendy, S. Lau, P. Teh, H. Lee, C. Tan, S. Ramesh, "Effects of anodisation parameters on thin film properties: A review", Mater. Sci. Technol. Vol. 33, No. 6, 2017, pp. 699-711.

[7] R. Menini, M. Farzaneh, "Elaboration of al2o3/ptfe icephobic coatings for protecting aluminum surfaces", Surf. Coat. Technol. Vol. 203, No. 14, 2009, pp. 1941-1946.

[8] Z. Ghalmi, M. Farzaneh, "Durability of nanostructured coatings based on ptfe nanoparticles deposited on porous aluminum alloy", Appl. Surf. Sci. Vol. 314, No. 2014, pp. 564-569.

[9] Y. Wang, L. Xia, J. Ding, N. Yuan, Y. Zhu, "Tribological behaviors of lubricants modified nanoporous anodic alumina film", Tribol. Lett. Vol. 49, No. 2, 2013, pp. 431-437.

[10] S. Chen, C. Kang, J. Wang, C. Liu, K. Sun, "Synthesis of anodizing composite films containing superfine al2o3 and ptfe particles on al alloys", Appl. Surf. Sci. Vol. 256, No. 22, 2010, pp. 6518-6525.

[11] I. Mohammadi, A. Afshar, S. Ahmadi, "Al2o3/si3n4 nanocomposite coating on aluminum alloy by the anodizing route: Fabrication, characterization, mechanical properties and electrochemical behavior", Ceram. Int. Vol. 42, No. 10, 2016, pp. 12105-12114.

[12] X.-Y. Lv, J.-W. Hou, Z.-X. Gao, H.-F. Liu, "Synthesis and characteristics of large-area and high-filling cds nanowire arrays in aao template", J. nanosci. nanotechnol. Vol. 18, No. 5, 2018, pp. 3709-3712.

[13] S. Ateş, E. Baran, B. Yazıcı, "The nanoporous anodic alumina oxide formed by two-step anodization", Thin Solid Films, Vol. 648, No. 2018, pp. 94-102.

[14] Y. Li, Y. Qin, S. Jin, X. Hu, Z. Ling, Q. Liu, J. Liao, C. Chen, Y. Shen, L. Jin, "A new self-ordering regime for fast production of long-range ordered porous anodic aluminum oxide films", Electrochim. Acta. Vol. 178, No. 2015, pp. 11-17.
[15] W.J. Stępniowski, A. Nowak-Stępniowska, A. Presz, T. Czujko, R.A. Varin, "The effects of time and temperature on the arrangement of anodic aluminum oxide nanopores", Mater. charact. Vol. 91, No. 2014, pp. 1-9.
[16] S. Akiya, T. Kikuchi, S. Natsui, N. Sakaguchi, R.O. Suzuki, "Self-ordered porous alumina fabricated via phosphonic acid anodizing", Electrochim. Acta. Vol. 190, No. 2016, pp. 471-479.
[17] W. Lee, "Structural engineering of porous anodic aluminum oxide (aao) and applications", 2015.
[18] A. O Araoyinbo, A. Iskandar Azmi, C. Mohd Ruzaidi Ghazali, A. Rahmat, K. Hussin, M. Mustafa Albakri Abdullah, "Nanoporous alumina fabrication: A short review", Nanosci. Nanotechnol.-Asia. Vol. 7, No. 2, 2017, pp. 183-199.
[19] J. ter Maat, R. Regeling, C.J. Ingham, C.A. Weijers, M. Giesbers, W.M. de Vos, H. Zuilhof, "Organic modification and subsequent biofunctionalization of porous anodic alumina using terminal alkynes", Langmuir. Vol. 27, No. 22, 2011, pp. 13606-13617.
[20] C.B. Gorman, R.J. Petrie, J. Genzer, "Effect of substrate geometry on polymer molecular weight and polydispersity during surface-initiated polymerization", Macromol. Vol. 41, No. 13, 2008, pp. 4856-4865.
[21] M. Pashchanka, J. Engstler, J.J. Schneider, V. Siozios, C. Fasel, R. Hauser, I. Kinski, R. Riedel, S. Lauterbach, H.J. Kleebe, "Polymer-derived sioc nanotubes and nanorods via a template approach", Eur. J. Inorg. Chem. Vol. 2009, No. 23, 2009, pp. 3496-3506.
[22] Y. Hu, M. Gu, X. Liu, J. Zhang, S. Huang, B. Liu, "Sol-gel template synthesis and characterization of lu2o3: Eu3+ nanowire arrays", Micromachines. Vol. 9, No. 11, 2018, pp. 601.
[23] K. Wang, P. Birjukovs, D. Erts, R. Phelan, M.A. Morris, H. Zhou, J.D. Holmes, "Synthesis and characterisation of ordered arrays of mesoporous carbon nanofibres", J. Mater. Chem. Vol. 19, No. 9, 2009, pp. 1331-1338.
[24] Y. Wang, M. Wu, Z. Jiao, J.Y. Lee, "One-dimensional sno2 nanostructures: Facile morphology tuning and lithium storage properties", Nanotechnol. Vol. 20, No. 34, 2009, pp. 345704.
[25] J. Zhou, J. He, P. He, H. Zhang, M. Tang, Y. Ji, X. Liu, W. Dang, "Ternary alloy ni–w–p nanoparticles electroless deposited within alumina nanopores", Mater. Sci. Technol. Vol. 24, No. 10, 2008, pp. 1250-1253.
[26] G. Wang, C. Shi, N. Zhao, X. Du, "Synthesis and characterization of ag nanoparticles assembled in ordered array pores of porous anodic alumina by chemical deposition", Mater. Lett. Vol. 61, No. 18, 2007, pp. 3795-3797.
[27] I.-W. Sun, J.-K. Chang, "Electrodeposition of nanomaterials", 2017.
[28] P.-S. Cheow, E.Z.C. Ting, M.Q. Tan, C.-S. Toh, "Transport and separation of proteins across platinum-coated nanoporous alumina membranes", Electrochim. Acta. Vol. 53, No. 14, 2008, pp. 4669-4673.
[29] W.-F. Hsu, C.-G. Kuo, Y.-C. Chao, J.-F. Lee, C.-F. Yang, F.-R. Juang, "Growth of zno nano-wire arrays using aao template and atomic-layer deposition method", Proc. 2016 International Conference on Applied System Innovation (ICASI), 2016, pp. 1-4.
[30] D.A. Brevnov, M.J. Barela, M.J. Brooks, G.P. López, P.B. Atanassov, "Fabrication of anisotropic super hydrophobic/hydrophilic nanoporous membranes by plasma polymerization of c 4 f 8 on anodic aluminum oxide", J. Electrochem. Soc. Vol. 151, No. 8, 2004, pp. B484-B489.
[31] E. Fleming, F. Du, E. Ou, L. Dai, L. Shi, "Thermal conductivity of carbon nanotubes grown by catalyst-free chemical vapor deposition in nanopores", Carbon. Vol. 145, No. 2019, pp. 195-200.
[32] S.J. Hurst, E.K. Payne, L. Qin, C.A. Mirkin, "Multisegmented one-dimensional nanorods prepared by hard-template synthetic methods", Angew. Chem. Int. Ed. Vol. 45, No. 17, 2006, pp. 2672-2692.
[33] W. Lee, R. Scholz, K. Nielsch, U. Gösele, "Titelbild: A template-based electrochemical method for the synthesis of multisegmented metallic nanotubes (angew. Chem. 37/2005)", Angew. Chem. Vol. 117, No. 37, 2005, pp. 6055-6055.
[34] P.G. Schiavi, P. Altimari, A. Rubino, F. Pagnanelli, "Electrodeposition of cobalt nanowires into alumina templates generated by one-step anodization", Electrochim. Acta. Vol. 259, No. 2018, pp. 711-722.
[35] W. Chen, S. Tang, M. Lu, Y. Du, "The magnetic properties and reversal of fe–co nanowire arrays", Journal of Physics: Condensed Matter, Vol. 15, No. 26, 2003, pp. 4623.

[36] D. Sellmyer, M. Zheng, R. Skomski, "Magnetism of fe, co and ni nanowires in self-assembled arrays", J. Phys.: Condens. Matter. Vol. 13, No. 25, 2001, pp. R433.
[37] T. Mehmood, A. Mukhtar, B.S. Khan, K. Wu, "Growth mechanism of electrodeposited fe, co and ni nanowires in the form of self-assembled arrays at fixed potential", Int. J. Electrochem. Sci. Vol. 11, No. 2016, pp. 6423-31.
[38] J. Liu, F. Wang, J. Zhai, J. Ji, "Controllable growth and magnetic characterization of electrodeposited nanocrystalline ni–p alloy nanotube and nanowire arrays inside aao template", J. Electroanal. Chem. Vol. 642, No. 2, 2010, pp. 103-108.
[39] Y. Xie, D. Kocaefe, C. Chen, Y. Kocaefe, "Review of research on template methods in preparation of nanomaterials", J. Nanomater. Vol. 2016, No. 2016, pp. 11.
[40] K. Ang, S. Venkatraman, R. Ramanujan, "Magnetic pnipa hydrogels for hyperthermia applications in cancer therapy", Mater. Sci. Eng. C, Vol. 27, No. 3, 2007, pp. 347-351.
[41] R. Jamaati, M.R. Toroghinejad, A. Najafizadeh, "Application of anodizing and car processes for manufacturing al/al2o3 composite", Mater. Sci. Eng. A, Vol. 527, No. 16-17, 2010, pp. 3857-3863.
[42] S.-J. Ma, P. Luo, H.-h. Zhou, C.-P. Fu, Y.-F. Kuang, "Preparation of anodic films on 2024 aluminum alloy in boric acid-containing mixed electrolyte", Trans. Nonferrous Met. Soc. China, Vol. 18, No. 4, 2008, pp. 825-830.
[43] X. Wang, G.-R. Han, "Fabrication and characterization of anodic aluminum oxide template", Microelec. Eng. Vol. 66, No. 1-4, 2003, pp. 166-170.
[44] C.H. Voon, B.Y. Lim, K. Foo, U. Hashim, S.T. Sam, M. Arshad, M. Khairuddin, N. Mustafa, "Synthesis of porous anodic alumina (paa) on aluminum alloy aa6061 in mixture of phosphoric acid and oxalic acid", Proc. Mater. Sci. Forum. 2016, pp. 237-241.
[45] I. De Graeve, H. Terryn, G.E. Thompson, "Influence of local heat development on film thickness for anodizing aluminum in sulfuric acid", J. Electrochem. Soc. Vol. 150, No. 4, 2003, pp. B158-B165.
[46] P.G. Sheasby, R. Pinner, The surface treatment and finishing of aluminium and its alloys, ed., ASM Int. 2001,
[47] C. Voon, M.N.B. Derman, U. Hashim, K. Foo, T. Adam, "Effect of anodizing voltage on the morphology and growth kinetics of porous anodic alumina on al-0.5 Wt% mn alloys", Proc. Adv. Mater. Res. 2014, pp. 101-106.
[48] T. Aerts, J.-B. Jorcin, I. De Graeve, H. Terryn, "Comparison between the influence of applied electrode and electrolyte temperatures on porous anodizing of aluminium", Electrochim. Acta. Vol. 55, No. 12, 2010, pp. 3957-3965.
[49] T. Aerts, T. Dimogerontakis, I. De Graeve, J. Fransaer, H. Terryn, "Influence of the anodizing temperature on the porosity and the mechanical properties of the porous anodic oxide film", Surf. Coat. Technol. Vol. 201, No. 16-17, 2007, pp. 7310-7317.
[50] K. Ng, Y. Lin, A. Ngan, "Deformation of anodic aluminum oxide nano-honeycombs during nanoindentation", Acta Mater. Vol. 57, No. 9, 2009, pp. 2710-2720.
[51] T.-H. Fang, T.H. Wang, S.-H. Kang, C.-H. Chuang, "Indentation deformation of mesoporous anodic aluminum oxide", Curr. Appl. Phys. Vol. 9, No. 4, 2009, pp. 880-883.
[52] A.H. Mahmud, A.S. Habiballah, A. Jani, "The effect of applied voltage and anodisation time on anodized aluminum oxide nanostructures", Proc. Mater. Sci. Forum. 2015, pp. 103-108.
[53] N. Hassanzadeh, H. Omidvar, "The effect of gradual decreasing the anodizing voltage on the morphology of alumina nanochannels", Researchgate.
[54] L. Bouchama, N. Azzouz, N. Boukmouche, J. Chopart, A. Daltin, Y. Bouznit, "Enhancing aluminum corrosion resistance by two-step anodizing process", Surf. Coat. Technol. Vol. 235, No. 2013, pp. 676-684.
[55] Y.-C. Kim, B. Quint, R.W. Kessler, D. Oelkrug, "Structural properties of electrochemically designed porous oxide films on almg1", J. electroanal. chem. Vol. 468, No. 1, 1999, pp. 121-126.
[56] G. Bertotti, Hysteresis in magnetism: For physicists, materials scientists, and engineers, ed., Academic press, 1998,
[57] C.H. Kim, Y. Myung, Y.J. Cho, H.S. Kim, S.-H. Park, J. Park, J.-Y. Kim, B. Kim, "Electronic structure of vertically aligned mn-doped $CoFe_2O_4$ nanowire and their application as humidity sensors and photodetectors", J. Phys. Chem. C, Vol. 113, No. 17, 2009, pp. 7085-7090.
[58] C. Pham-Huu, N. Keller, C. Estournes, G. Ehret, M. Ledoux, "Synthesis of $CoFe_2O_4$ nanowire in carbon nanotubes. A new use of the confinement effect", Chem. Commun. Vol. No. 17, 2002, pp. 1882-1883.
[59] S.M. El-Sheikh, F.A. Harraz, M.M. Hessien, "Magnetic behavior of cobalt ferrite nanowires

prepared by template-assisted technique", Mater. Chem. Phys. Vol. 123, No. 1, 2010, pp. 254-259.
[60] T. Prabhakaran, R. Mangalaraja, J.C. Denardin, J. Jiménez, "The effect of reaction temperature on the structural and magnetic properties of nano $CoFe_2O_4$", Ceram. Int. Vol. 43, No. 7, 2017, pp. 5599-5606.
[61] X.-y. HOU, J. FENG, X.-h. LIU, M.-l. ZHANG, "Comparable studies of adsorption and magnetic properties of ferrite $MnFe_2O_4$ nanoparticles, porous bulks and nanowires", Chem. Res. Chinese Uni. Vol. 27, No. 4, 2011, pp. 543-546.
[62] H.-J. Cui, J.-W. Shi, B. Yuan, M.-L. Fu, "Synthesis of porous magnetic ferrite nanowires containing mn and their application in water treatment", J. Mater. Chem. A, Vol. 1, No. 19, 2013, pp. 5902-5907.
[63] L. Malkinski, J.-H. Lim, W.-S. Chae, H.-O. Lee, E.-M. Kim, J.-S. Jung, "Fabrication and magnetic properties of $MnFe_2O_4$ nanowire arrays", Elec. Mater. Lett. Vol. 5, No. 2, 2009, pp. 87-90.
[64] S. Liu, B. Yue, K. Jiao, Y. Zhou, H. He, "Template synthesis of one-dimensional nanostructured spinel zinc ferrite", Mater. Lett. Vol. 60, No. 2, 2006, pp. 154-158.
[65] Y. Li, Y. Huang, L. Yan, S. Qi, L. Miao, Y. Wang, Q. Wang, "Synthesis and magnetic properties of ordered barium ferrite nanowire arrays in aao template", Appl. Surf. Sci. Vol. 257, No. 21, 2011, pp. 8974-8980.
[66] Z. Hua, R. Chen, C. Li, S. Yang, M. Lu, B. Gu, Y. Du, "$Cofe_2o_4$ nanowire arrays prepared by template-electrodeposition method and further oxidization", J. alloy. compd. Vol. 427, No. 1-2, 2007, pp. 199-203.